The Effects of Electrical Microstimulation on Cortical Signal Propagation

Nikos K Logothetis, Mark A Augath, Yusuke Murayama, Alexander Rauch, Fahad F Sultan, Jozien Goense, Axel Oeltermann, Hellmut Merkle

The Effects of Electrical Microstimulation on Cortical Signal Propagation

Logothetis, N.K[1, 2,*], Augath, M[1,*], Murayama, Y[1,*], Rauch, A[1], Sultan, F[3], Goense, J[1], Oeltermann, A[1], and Merkle, H[4]

MAX PLANCK INSTITUTE FOR BIOLOGICAL CYBERNETICS

1) Max Planck Institute for Biological Cybernetics, Tuebingen, Germany

2) Imaging Science and Biomedical Engineering, University of Manchester, Manchester, United Kingdom

3) Hertie Institute for Clinical Brain Research, Dept. Cognitive Neurology, University Tuebingen

4) NINDS, Lab Funct & Mol Imaging, NIH, Bethesda, MD 20892 USA

* These authors made equal contributions to the work.

Corresponding Author: Nikos K. Logothetis
Spemannstr 38
72076 Tübingen
Germany
Tel: +49 7071 601-650
Fax: +49 7071 601-660
Email: nikos.logothetis@tuebingen.mpg.de

Keywords: Monkey, Cortical Microstimulation, fMRI, Signal Propagation, Cortical Microcircuits, Inhibition, Recurrence

Electrical stimulation (ES) is used in animals and humans to study potential causal links between neural activity and specific cognitive functions. Recently, it has found increased application in electrotherapy and neural prostheses as well. However, how ES-elicited signals propagate in brain tissues is still unclear. Here we used combined electrostimulation, neurophysiology, microinjection and fMRI to study the cortical activity patterns elicited during stimulation of cortical afferents in monkeys. We find that stimulation of a site in LGN (lateral geniculate nucleus) increases the fMRI signal in the regions of primary visual cortex (V1) receiving input from that site, but suppresses it in the retinotopically matched regions of extrastriate cortex. In agreement with previous observations, intracranial recordings show that immediately after a stimulation pulse a long-lasting inhibition follows a short excitatory response. Following microinjections of GABA (γ-aminobutyric acid) antagonists in V1, LGN stimulation induces positive fMRI signals in all cortical areas. Taken together, our findings suggest that ES disrupts cortico-cortical signal propagation by silencing the output of any neocortical area whose afferents are electrically stimulated.

We recently developed and optimized the esfMRI (combined ES and fMRI) methodology for experiments in anesthetized and behaving monkeys[1, 2]. Our first experiments, including fMRI-based estimations of tissue excitability (rheobase and chronaxie measurements), showed that electrical stimulation of the primary visual cortex V1 mainly excites large pyramidal cells and axons, eliciting positive BOLD responses (PBR) in topographically matched regions of extrastriate areas such as V2, V3, V3A, V4, and MT (V5); all monosynaptic targets of the primary visual cortex. These findings are consistent with the well-established anatomical connections between V1 and the extrastriate cortex of macaque monkeys[3]. One puzzling observation in our initial studies was the clear lack of transsynaptic effects during cortical stimulation. In the present study, we stimulated either the LGN or the pulvinar (Pul) in anesthetized and alert monkeys in order to systematically examine the propagation of ES-induced signals.

We demonstrate that electrical stimulation of a thalamic site indeed suppresses the neural activity of its projection regions in visual cortex. The strong reduction in BOLD response is likely due to synaptic inhibition and it be can be reversed by injections of GABA antagonists in V1. In agreement with the fMRI results, intracortical recordings show that an electric pulse evokes an action potential followed by a pronounced and long-lasting inhibition. Such disruptive effects of cortical afferent stimulation on the activity of projection neurons have already been reported. Yet, by using the combined physiology, pharmacology and fMRI approach here we illustrate for the first time the extent and generality of ES-induced activity suppression, and we propose that many behavioral effects that were obtained over the years by means of electrical stimulation of the afferents of sensory or association cortical areas may be largely mediated by cortico-subcortico-cortical pathways.

BOLD RESPONSES TO ELECTRICAL STIMULATION OF THALAMUS

The present study involved 53 combined microstimulation-fMRI experimental sessions in 8 healthy anesthetized monkeys (Macaca mulatta) and 37 corresponding sessions in two trained awake monkeys. Thirty-nine out of 53 anesthetized sessions were included in the data analysis; the rest were devoted to the development of the stimulation and microinjection techniques. Brain activity during ES was measured with BOLD fMRI in a 4.7 T/40 cm and a 7 T/60 cm magnet in anesthetized and alert animals, respectively. Detailed protocols of electrostimulation, BOLD fMRI and physiology are described in a number of publications[2, 4, 5] as well as in the online methods of this paper. Briefly, in each experimental session, the stimulation electrode (iridium) was advanced to the desired location, the receptive field (RF) in each LGN layer was mapped, and the stimulation site was selected so as to ensure reliable electrically evoked BOLD activation on the operculum of the brain. In three

animals (2 for anesthetized, 1 for alert studies), the electrodes were implanted permanently at the end of the site-selection process.

Electrical stimulation of the LGN elicited robust PBR in LGN itself and in superior colliculus (SC), Pul, and V1 as shown by the thresholded t-statistic maps in **Figure 1a**. Red regions indicate voxels with ES-induced, positive BOLD responses; their average time courses are illustrated in **Figure 1b**. In contrast to V1, the extrastriate areas V2, XC and V5 (MT) showed large negative BOLD responses (NBR). The term XC refers to the early extrastriate areas beyond V2, that is the areas V3, V3A, V4, V4t and posterior TEO, which were reliably deactivated during the electrical stimulation of V1 afferents. The stimulus-induced activations were mapped using a general linear model (GLM[6]).

Figure 1c and **1d** show respectively the activation maps and time courses obtained following pulvinar stimulation. Robust PBR were observed in LGN, SC, Pul, and V1. In sharp contrast to the LGN, however, the electrical stimulation of the pulvinar induced signal increases in V2 and all extrastriate areas (XC: V3, V4, TEO) and V5 (MT) **(Fig. 1c)**. At first glance, this might appear to contradict the results of LGN stimulation, but it does not; the ES-induced activation of extrastriate cortex merely reflects the connectivity of the latter with higher (association) thalamic nuclei; a large number of cortical visual areas indeed directly (monosynaptically) connect with pulvinar. In fact, it has been suggested that for every corticocortical connection there is a "replicating" cortico-pulvinar-cortical linkage[7], and that a subset of direct driver corticocortical pathways transmits information between cortical areas in parallel with cortico-thalamo-cortical pathways involving higher order thalamic nuclei[8]. The activations observed during the electrical stimulation of pulvinar stimulation likely occur by means of these monosynaptic pulvinar-extrastriate-cortex connections.

Sustained cortical NBR have been reported during sensory stimulation and were shown to reflect regional decreases in neuronal activity below spontaneous activity[9]. They typically occur near the cortical regions that are directly activated by sensory stimulation and likely reflect lateral or top-down cortical interactions during sensory stimulation[9]. To dissect such NBR from the deactivation patterns presented here, we used an experimental paradigm that permits the examination of ES-induced responses exclusively within regions showing PBR during visual stimulation.

To do this we alternated large-field visual and electrical stimulation of LGN by first mapping voxels with positive BOLD responses during visual stimulation (vPBR) and subsequently examined the distribution of ES-induced PBR and NBR within the vPBR regions (Fig. 2). With this mixed design, stimulus-induced activations were obtained by using an inclusive (restrictive) GLM, whereby the electrically induced positive and negative responses were exclusively confined within the PBR regions mapped during visual stimulation. Almost all ES-modulated regions in subcortical structures and V1 exhibited robust PBR, while those in V2 and XC were deactivated. One exception was area MT, in which the response sign depended on electrode position, most likely reflecting the extent to which the koniocellular system was activated by electrical stimulation[10]. This hypothesis is supported by the fact that in animals with implanted electrodes the MT response was consistent from experiment to experiment; one animal showed decreases and two showed increases in the BOLD response. Figure 2c illustrates the results of concurrent visual and electrical stimulation. In this experimental design, a 10 s blank period was followed by 10 s visual stimulation (rotating checkerboard), then 10s of combined visual and biphasic electrical stimulation, 10 s visual stimulation alone, and finally 10 s post-stimulus blank. This sequence was repeated 6 times during each MR scan and had a total of 5 min duration. The time course of the signal is the average of all voxels in the activated or deactivated regions that were selected with the GLM of the sequential

design shown in **Figure 2b.** Note that the addition of the electrical stimulus further enhances V1 responses, while it profoundly decreases the V2 BOLD responses.

Figure 3 shows the stimulation sites and population BOLD responses (N=32 sessions) to visual and electrical stimulation of LGN and pulvinar. Three-dimensional reconstructions **(Fig. 3b)** and flat maps **(Fig. 3c)** illustrate the location and extent of activations and deactivations during electrical stimulation of LGN and pulvinar; average time courses are displayed in **Figure 3d**. On the whole, electrical stimulation of the afferents of a cortical region activates that region (the vast majority of significantly modulated V1 voxels show PBR) while strongly suppressing the activity of subsequent processing stages (97% of significantly modulated XC voxels show NBR, for instance). Similarly, the stimulation of pulvinar activates all monosynaptic targets, which in this case include the robustly modulated regions of V1, XC, and MT.

Interestingly, stimulation of LGN consistently activated superior colliculus and pulvinar, even though neither structure receives direct LGN input. The SC BOLD responses could be the result of activation of the Meynert cells of the deep cortical layers (V and VI) of V1 which are known to project to SC. Given that these very same layers receive monosynaptic input from LGN, it is reasonable to assume that ES propagates through the LGN-V1-SC pathway. Corticofugal paths might also underlie the activation of pulvinar. Cortico-pulvinar output arises from layer Vb of V1, and pulvino-cortical feedback to V1 terminates mainly in layer 1. Thus, the activation of pulvinar may also be due to the LGN-V1-pulvinar pathway.

Figure 4 – Alert Monkey: Single Session & Population

LGN was also stimulated in 37 sessions in two awake monkeys performing fixation tasks (online methods). The spatial resolution in these experiments was usually 1x1 mm^2 (with a few sessions with 0.75x0.75 mm^2 in plane resolution). Electrical stimulation of LGN typically induced activation of the primary visual cortex and negative BOLD response in the extrastriate cortex (Fig. 4 and Supplementary Fig. 1). Overall, 95.7% of the (significantly modulated) V1 voxels showed PBR and 98.2% of the V2 voxels NBR to electrical stimulation ($p<0.0001$, uncorrected), demonstrating that the observed deactivations are unrelated to the opiates used in experiments with anesthetized monkeys.

EFFECTS OF CURRENT STRENGTH AND PULSE FREQUENCY ON BOLD

ES-induced fMRI is only possible if a sufficiently large population of neurons is activated to evoke a measurable hemodynamic response. To obtain robust and reproducible activation maps, most of our experiments used biphasic pulses of 200 µs duration and 250 µA strength, delivered at 200 Hz with large-surface electrodes (100 µm Ir with a typical tip surface of A=0.006 mm^2) yielding relatively low charge density (833 $\mu C/cm^2$, see also online methods). The latter denotes the current-intensity-driven charge flow over the pulse-duration time and per electrode surface area (current multiplied with duration and divided by surface), and it is comparable with other microstimulation-physiology studies using lower current intensities. In a study of intracortical stimulation in rats[11], for instance, currents of 20 µA and 500 µs duration were injected via an electrode of 0.00114 mm^2 surface, yielding 877 $\mu C/cm^2$. Nonetheless, we also systematically tested fMRI activations using different current strengths and pulse frequencies.

In V1 the activated volume shrank systematically as the intensity of the current decreased **(Supplementary Fig. 2a)**, while in the extrastriate cortex there was no clear trend, barring the case of the lowest current intensity. **Supplementary Fig. 2b** shows cortical sites with significant activity changes under all stimulation conditions

(logical "AND" operation), and **Supplementary Fig. 2c** displays their time courses for pulses of different current strengths. At all intensities (10, 20, 30, 50, 100 μA, 200 Hz, biphasic pulses of 200 μs duration) there is clear activation in V1 and deactivation in the extrastriate cortex.

In contrast, both sign and amplitude of the V1 (monosynaptic target of LGN) BOLD responses depended on stimulation frequency (Fig. 5a). As with sequential electrical and visual stimulation of the LGN (Fig. 2), with 200 Hz stimulation the ROI in V1 shows PBR and that in V2 shows NBR. The lower plot shows exactly the same ROI for visual and 12 Hz electrical stimulation. Now, a striking negative BOLD response is seen in the V1 ROI, accompanied by strong V2 deactivation. When visual and electrical stimuli were used in combination **(Fig. 5b)**, the fMRI response in the V1 ROI was strongly reduced below baseline activity, similar to what was observed in the V2 ROI.

The frequency effects on V1 BOLD responses are shown in more detail in **Figure 5c**. The left panel displays the thresholded t-statistic maps ($p<0.0001$, uncorrected). Here, too, red and blue illustrate significantly modulating voxels in V1 and V2 respectively, during sequential visual and electrical (200Hz) stimulation. The time courses of these two ROI are shown at right for stimulation with pulses of different frequencies. High frequencies (e.g. 100 Hz, 200 Hz) yielded robust PBR in the V1 ROI, while at low frequencies (lower than 50-70 Hz) the same ROI showed consistent negative BOLD responses, the amplitude of which reached a maximum at about 10-12 Hz. BOLD responses in the V2 ROI were always negative (tested frequency range 1-800 Hz – data not shown).

NEURAL RESPONSES TO SINGLE ELECTRICAL PULSES

We examined the neural origin of these BOLD signal changes by conducting a number of concurrent electrophysiology and fMRI experiments as well as experiments with electrode arrays outside of the magnet. Recordings were mainly done in the operculum of the primary visual cortex during LGN stimulation. Previous in vitro and in vivo intracellular and extracellular studies[12-15] demonstrated that during the stimulation of cortical afferents or cortex, single electrical pulses are typically followed by a sequence of excitation and inhibition, the dynamic properties of which are best explained by the organization of cortical microcircuits[12]. Indeed, in our experiments, too, a single bi-phasic stimulus pulse in LGN often induced in V1 a sequence of very short excitation followed by a long-lasting inhibition (100-300 ms) that occasionally completely eliminated any spontaneous action potential discharge **(Fig. 6a)**. The full recovery period was often as long as 500 ms. But occasionally, multiunit responses were also characterized by only a brief excitation.

To quantify these results, the spiking responses of all sessions were partitioned into subsets using a standard unsupervised learning method, (the k-means algorithm). The number of clusters used for classification was determined based on a preliminary PCA (principle component analysis), indicating that three temporal profiles explain over 75% of the variance of cortical responses during thalamic stimulation (**Fig. 6b**). Clustering was optimized by excluding the strong phasic response immediately following an electrical pulse (10 msec) from the data (e.g. gray transparent rectangles in **Fig. 6c**). Application of the k-means algorithm with a *cosine* distance (one minus the cos of the angle between points treated as vectors) as similarity measure yielded three response types (**Fig. 6c**): the first two included long (45%) and short (20%) lasting inhibitory responses and the third brief excitatory (35%) responses. **Figure 6d** depicts the power of the low (1-40 Hz, thick lines) and high (60-100 Hz, thin lines) frequency ranges of the LFP for all recording sites clustered on the basis of spiking activity. Interestingly, different response types were frequently observed at different cortical depths. **Figure 6e** shows the average recording position (distance from the pial surface) for all three clusters. Depth differences between clusters 1 and 3 ($p<0.0002$) were significant, suggesting that long-lasting inhibitory responses might be

predominantly initiated in the superficial layers of cortex. In contrast, brief excitatory responses (cluster 3) appeared to occur more often in the lower cortical layers.

We further examined the dynamics of the long inhibition characterizing the majority of responses (cluster 1) by calculating the time-to-peak, amplitude and time constant (Tau) of each recording site's average response, fitting an inverted gamma function to the data and computing the time and amplitude of the curve minimum, as well as the time point at which the inhibitory response had recovered by 73% of the maximum inhibition. On average each electrical pulse reduced spiking by 40-70% of the baseline level at about 20-50 ms after the pulse **(Supplementary Fig. 3a)**. Maximum inhibition increased with increasing current strength, but it was followed by a slow recovery with a Tau value of approximately 150-200 ms independent of current strength **(Supplementary Fig. 3b-d)**. This result is in agreement with previous studies applying electrical stimulation in the somatosensory cortex of rats and mice[15, 16].

To better understand the remarkable effects of stimulation frequency on the V1 BOLD responses, we calculated two parameters of the single-pulse responses: (a) the pulse efficiency, i.e. the probability of a spike response after each electrical pulse, and (b) the average inter-pulse spiking activity. We first assessed the magnitude and duration of electrical artifacts introduced by stimulation inside and outside of the scanner. Initial measurements were conducted in a saline bath. During stimulation each electric pulse resulted in an initial saturation of the amplifying system. The saturation settled down monotonically to baseline typically within 0.5-1 ms without any additional artifacts, mainly due to the fact that the current source utilized for stimulation created an electric field only during current application. This stimulation is similar in the brain as a consequence of the purely resistive properties of the volume conductor[17]. Spike latency was found to be in the range of 1.8-3.5 ms. Pulse efficiency was therefore estimated from peristimulus histograms of 1 ms bin width, by excluding one bin before and after the stimulus pulse and dividing the number of spikes within 1-4 ms after each pulse by the number of pulses. Inter-pulse spiking activity was estimated by averaging spiking within each time window from 6 to 10 ms, or for the period from 6 ms after a pulse to the next pulse; the two measures yielded similar results, and were used to compare inhibition during low and high frequency stimulation. **Figure 6f** shows the efficiency of each pulse for different stimulation frequencies. Interestingly, pulse efficiency was found to depend non-monotonically on stimulation frequency, with a minimum in the range of 4-12 Hz. Indeed, stimulation around these frequencies appears to have the greatest suppressive effect on both thalamocortical and intracortical activity (see also[13-16]). **Figure 6g** depicts the percent change in firing rate for the inter-pulse intervals with respect to the pre-stimulus baseline spiking. Firing rate, here reflecting the overall microcircuit activity between successive pulses, rises above baseline only with frequencies around and above 100 Hz.

EFFECTS OF GABA ANTAGONISTS ON ES-INDUCED BOLD RESPONSES

These physiology results showed that each stimulation pulse in LGN induces strong cortical inhibition with a prolonged recovery period lasting several hundred milliseconds that is largely independent of stimulus strength. Moreover, intracortical stimulation in mice and rats has shown that the duration of inhibition following a single electrical pulse remains unaffected by a following second pulse; a fact suggesting that depression of spiking activity may be due to synaptic inhibition rather than excitability changes[16].

To further test the hypothesis that the deactivation of extrastriate cortex might be due to synaptic inhibition of V1 projection neurons, we microinjected GABA antagonists into V1 in experiments combining fMRI, electrophysiological recordings, and microstimulation. GABAergic action was blocked with a solution of bicuculline methiodide (BMI) that was slowly injected into V1 (methods). The injections were delivered at depths

corresponding to cortical layers IV/V, typically within a region (INJ) extending a few millimeters from the injector **(Fig. 7a)**. The injection projection zone (IPZ), the area receiving direct connections from INJ, was estimated by sparse retinotopic mapping; small rotating polar checkerboard stimuli were placed in a visual field position that elicited visual BOLD responses around the tip of the injector. The V2 activation induced by such stimuli was considered to indicate the IPZ. In sessions in which no sparse retinotopic mapping was done, IPZ was initially estimated by the known retinotopic organization of the early visual areas (e.g.[18]).

We identified the injection-related activation patterns by first decomposing the BOLD data for each session into a set of independent components (ICs, n=20) using spatial ICA (independent component analysis; for details see **Supplementary Fig. 4** and online methods). Relevant ICs were selected based on significant ES-induced modulation in the pre-injection period[19]. In the majority of experimental sessions, four prominent components were evident **(Supplementary Fig. 4a)**. One IC was mainly localized around the injector (INJ region), which exhibited a strong baseline shift and a peak in its time course 9-12 minutes after the BMI injection **(Supplementary Fig. 4b)**. Two ICs were found with no baseline shifts and a time course characterized by ES-induced modulation that was correlated (V1) or anticorrelated (V2) with the electrical stimulus, and another IC with a baseline shift and characterized by negative ES-induced BOLD responses in the pre-injection period and positive responses shortly after the injection. Based on their strong inter-session similarity, we included the average time courses of the INJ and IPZ clusters over all sessions as regressors for the GLM. The population results from the injection experiments (Fig. 7) show that within the IPZ RO1, there is a clear response inversion following the injection of the GABA antagonist. The dynamics of the response inversion after the injection can be seen in **Fig 7d**, in which the coefficient of correlation between stimulus and BOLD response for each trial (stimulus-blank) is plotted as a function of time. A few minutes after injection of BMI the correlation coefficients become positive, indicating the positive BOLD responses in INJ.

DISCUSSION

Here, we demonstrated that electrical stimulation of a thalamic site suppresses the neural activity of its projection regions in visual cortex **(Supplementary Fig. 5a)**. The magnitude of suppression depends on stimulation frequency, with strongest deactivations (NBR) occurring in the 10-24 Hz range. For stimulation frequencies above 60 Hz, cortical regions that are polysynaptically connected to LGN continue to show NBR; monosynaptic LGN targets, however, show strong positive BOLD responses (PBR). These effects are independent of current strength and are consistently observed with currents as low as 10 μA.

Intracortical recordings in V1 showed that an electric pulse typically evokes an action potential followed by a pronounced and long-lasting inhibition, which occasionally completely eliminates any spontaneous spiking within the inter-pulse interval. Pulse efficiency, (the probability of a pulse initiating an action potential), depends non-monotonically on stimulation frequency, with a minimum in the frequency range of 2-12 Hz, within which inter-pulse spontaneous activity may drop to as much as 80% below baseline. Assuming that the first spike after stimulation is primarily due to thalamic input (see also[12-14]), the pulse efficiency reflects the activity of thalamocortical synapses to some extent. Consequently, the frequency dependence of BOLD signal in monosynaptic LGN targets may also be due to the activity of thalamocortical synapses as well as the spiking of cortical input neurons. Finally, LGN stimulation following injection of GABA antagonists in V1 induces PBR in both mono- and polysynaptic cortical targets of LGN **(Supplementary Fig. 5a)** suggesting that deactivations in extrastriate cortex are likely due to synaptic inhibition of efferents of V1.

Stimulation of LGN consistently activated superior colliculus and pulvinar, even though neither structure receives direct LGN input. In principle, SC BOLD responses could be mediated by antidromic stimulation of either retinal or cortical cells. Yet, a recent study in which the LGN of monkeys was stimulated during the execution of a sequential double-saccade task provided evidence arguing against such a thalamo-retino-tectal signal propagation[20]. Alternatively, SC BOLD may result from the activation of the Meynert cells of the deep cortical layers of V1 that project to SC[21]. Given that these very same layers receive monosynaptic input from LGN[22], it is reasonable to assume that the observed SC activations propagate through the LGN-V1-SC pathway. Similarly, cortico-pulvinar output arises from layer Vb of V1 (see review[7] and references therein), and antidromic activation of cells in these layers may propagate the ES-induced signal from LGN to pulvinar via cortex, despite the strong suppression of cortico-cortical signals at the supragranular layers. It should be noted that high frequency, neuronal element specific, optical stimulation (90 to 130 Hz) experiments have recently suggested that the antidromic stimulation of the afferents of the subthalamic nucleus (STN) – the main target of deep brain stimulation (DBS) – is the only optogenetic intervention that robustly ameliorated PD symptoms in hemiparkinsonian mice[23].

The disruptive effects of cortical afferent stimulation on the activity of projection neurons have already been reported, and they have even been exploited occasionally as a clever work-around for isolating specific cortical cell types. ES-induced microcircuit suppression in the primary visual cortex was used, for instance, for the study of the physiological properties of stelate neurons in isolation[13, 14]. But none of these studies explicitly discussed the fact that the structure and dynamics of microcircuits severely constrains the use of ES for the study of connectivity or behavior, or in electrotherapy and prosthetics. Indeed, the importance of the present work lies primarily in the very fact that the combined physiology, pharmacology and fMRI approach illustrates for the first time the extent and generality of ES-induced activity suppression, suggesting that many behavioral effects that were obtained over the years by means of electrical stimulation of the afferents of sensory or association cortical areas may be largely mediated by cortico-subcortico-cortical pathways.

At the level of individual cortical neurons, inhibition is ubiquitous and electrically inseparable from excitation[24-26]. One critical difference between sensory and electrical stimulation lies in the magnitude of inhibition, which in turn is affected by the temporal patterns of input potentials. In the case of sensory stimulation, inhibitory postsynaptic potentials lag behind the excitatory ones[27], but during the ES of afferents the premature feedforward and recurrent inhibition could readily block the weak thalamic input. The characteristic, intrinsic connectivity of cortical microcircuits has been demonstrated in many physiological, immunohistochemical and pharmacological experiments which found that axonal collaterals of the pyramidal cells often ascend back to and synapse in the superficial layers, while others distribute excitation in the horizontal plane, forming a potent recurrent excitatory network (see e.g. [28]). The strong amplification of the input signal caused by this kind of positive feedback loop is tightly controlled by a large variety of GABAergic interneurons[29] that are interposed within this pyramidal network.

Such recurrent microcircuits are by no means specific to sensory cortices; they have been evident wherever they have been sought, including the primary motor and premotor cortices in every mammal that has been studied so far[30, 31]. A characteristic example of excitatory-inhibitory interaction in neocortex, including motor, sensory and association areas, is the so-called frequency-dependent disynaptic inhibition. Under certain conditions, cortical pyramidal cell spiking drives specific classes of interneuronal populations, e.g. Martinotti cells, which in turn inhibit the apical and tufted dendrites of pyramidal cells[32]. Optimal operation of recurrent microcircuits is only ensured with spatio-temporally structured input patterns that – first and foremost – respect synaptic delays. ES violates this principle and consequently silences the output of neocortex, whether it is visual, auditory, or

somatosensory, whether stimulation is applied in thalamus or the clinically important basal ganglia, or whether ES is applied in mice, rats or higher mammals.

Scientists have been applying ES in humans and animals for over 100 years now, and although some might say it is a crude approach to studying the detailed mechanisms underlying various neural computations, there is no doubt that microstimulation has made significant contributions to our knowledge in both basic and clinical research. For example, ES has been extensively used to causally link the activity of various brain regions to perception and action, and recently it found application in electrotherapy and neural prostheses as well (for reviews see[33]). In animal experiments, ES was found to affect the decisions of animals involved in perceptual tasks[34, 35]. It has also enabled the investigation of projective fields[36] and offered insights into dynamic connectivity[37, 38]. Our present findings by no means contradict such studies, but they might recast or usefully constrain interpretations assuming normal cortico-cortical signal propagation. One example is a recent series of elegant experiments by Moore and colleagues, who found that subthreshold microstimulation of the FEF (frontal eye fields) enhances retinotopically corresponding V4 responses to isolated stimuli[39] and that the spatial signals involved in saccade preparation are used to covertly select from among multiple stimuli appearing within the RFs of visual cortical neurons[40]. These observations support the idea that FEF stimulation drives covert attention and its neural correlates in visual cortex[38, 40]. Microstimulation of the FEF, however, could recruit a number of different neural pathways. One possibility is that the reported enhancement of spike rate in V4 results from the electrical activation of the FEF neurons that project directly to that area[41]. Alternatively, modulations might be mediated by intervening areas (multisynaptic signal propagation) in frontal, parietal or subcortical brain regions[42]. Our current findings make paths through intervening cortical areas unlikely, leaving monosynaptic feedback or connections through SC and pulvinar as potential routes for the FEF-V4 interactions. Such cortico-subcortico-cortical (CSC) pathways through SC or pulvinar might also be the origin of activations induced by TMS in human TMS-fMRI studies[43]. Similarly, CSC pathways may underlie the activation patterns observed in monkey fMRI experiments examining the nature of FEF cortical connections[44, 45]. It is worth noting that both SC and pulvinar are known to be operative in spatial attention, and the physiology and connectivity of the latter makes it an exquisite route for indirect transcortical communication[7, 46].

Interestingly, the majority of investigators in cognitive science have long assumed that TMS (transcranial magnetic stimulation), the non-invasive stimulation of brain tissue by means of electromagnetic induction (Faraday's principle) and eddy (Foucault) currents, acts like a temporary "virtual lesion", since it disrupts neural processing in many different sensory, association or motor areas[47]. TMS of the cerebral cortex in fact exerts both excitatory and inhibitory effects on neural activity, the relative predominance of either type of effect being dependent on the timing of delivery, the strength, and the temporal structure of the TMS pulse sequences[48]. Such effects have been demonstrated with neurophysiological methods in the cat visual system, where TMS was found to inhibit the firing rate of stimulus-selective neurons[49]. In so-called repetitive TMS (rTMS), the pulse frequency ranges from 1-50 Hz, with 10 Hz being the frequency most frequently used in cognitive neuroscience[47]. On the basis of our findings we now assume that at that frequency the inhibition of the areas whose fibers were excited by TMS will be maximal, and in combined TMS and fMRI experiments using such frequencies, deactivations will be visible in both the monosynaptic and multisynaptic targets of the activated fibers. The fMRI activation and deactivation patterns that have been reported for TMS of different pulse frequencies in combined TMS-fMRI experiments[50] may be better understood in light of the frequency-dependent findings presented in this study.

Taken together, the findings reported in this study suggest that stimulation of cortical afferents disrupts the propagation of cortico-cortical signals after the first synapse. This conclusion is based on results obtained with

both anesthetized and alert animals. Yet, since the awake monkeys were involved in a simple fixation task only, one might argue that the activation/deactivation patterns may be different in subjects involved in cognitive tasks. The brief discussion of microcircuit organization above suggests that this is unlikely to be the case. Even if a cognitive state (e.g. attention or short-term memory) changed the ES-induced fMRI modulations of a given area by increasing or decreasing its level of excitation-inhibition balance, it would not alter the effects of ES on that area's output. To the best of our knowledge, long-range interactions between areas, e.g. fronto-parietal influences on sensory cortices, in all higher mammals occur through excitatory connections, rather than – for example – via inhibitory connections selectively targeting the interneurons of sensory cortices. The disruption of signal propagation simply reflects the synaptic organization of microcircuits and their response to an unnatural spatiotemporal input organization, and it would not be altered by either top-down effects or neuromodulation. The results obtained with electrical or transcranial magnetic stimulation may therefore need to be interpreted as showing either what an area does by itself together with all its subcortical projections (e.g. providing insights into the role of cortico-thalamo-cortical pathways, e.g. see **(Supplementary Fig. 5b)** or what kind of behaviors follow the reduction of activity in the monosynaptic targets of the stimulated region.

ACKNOWLEDGEMENTS

We thank Drs. Christoph Kayser, Oxana Eschenko, and Matthias Munk for reading the manuscript and for useful suggestions. Many thanks also go to Diane Blaurock for English corrections and editing, Stefan Weber for fine-mechanic work, and Thomas Steudel and Pedro Douay for help with the alert monkey experiments. This research was supported by the Max Planck Society, the German Research Foundation (DFG SFB-A9), and in part (HM) by the intramural research program of the NIH (National Institute Neurological Disorders and Stoke).

AUTHOR CONTRIBUTIONS

N.K.L. conceived the project, designed and supervised the experiments under anesthesia, analyzed the data, and wrote the paper, M.A. and Y.M. conducted the experiments, A.R. designed and conducted the pharmacology experiments, F.S. helped with flat map reconstructions, J.G. and Y.M. conducted the alert monkey experiments, and A.O. and H.M. developed and optimized the data acquisition and microstimulation hardware, and radiofrequency coils respectively.

FIGURES

Figure 1: Effects of thalamic microstimulation on the primary and extrastriate cortices (LGN **(a, b)**: animal F05, session *F05bf1*, Pulvinar **(c, d)**: animal D04, session *D04zn1*). **(a)** T-statistic maps thresholded at $p < 0.001$ (uncorrected, followed by cluster analysis). The cross in the 3rd slice shows the location of the microelectrode tip. Red indicates significant positive and blue significant negative signal changes. Robust positive responses are only observed in LGN, SC, Pul, and V1. In contrast, within the extrastriate areas V2, V3, V4, and V5 (MT) all significantly modulated voxels show large negative BOLD responses. Imaging parameters: echo-planar imaging (EPI), TE/TR=14.5/500 ms, FA=30 deg, FOV= [96x96] mm, M= [128x128x8], voxel size= [0.75x0.75] mm, slice: 2mm, volume TR = 1000 ms. Microstimulation parameters: 100 Hz biphasic pulses of 200 µs duration and 450 µA current intensity. An observation period consisted of 16 repetitions of a blank-microstimulation-blank trial with 4, 4, and 12 seconds duration, respectively. S1-S8: Slices 1 through 8. **(b)** The time course of the BOLD fMRI responses in different visual structures. Red and blue lines show positive and negative responses, respectively. The shaded areas indicate the 1% confidence interval (bootstrap estimate of the mean from 1000 samples). Shaded rectangles show the period of electrostimulation delivery. XC: extrastriate cortex approximately

including the areas V3, V3A, V4, and V4t. Colored contours indicate ROIs including different structures. V1, XC, MT, and subcortical structures, are depicted by yellow, cyan, orange and green contours respectively. The ordinates of the figures are in units of the standard deviation computed for the pre-stimulus interval, thus showing the functional signal-to-noise ratio (SNR) of the scan. **(c)** T-statistic maps thresholded at $p < 0.001$ (uncorrected) for pulvinar stimulation. The cross in the 5th slice shows the location of the electrode tip. **(d)** Time course of the BOLD fMRI responses during pulvinar stimulation in different visual structures. Imaging and microstimulation parameters as well as the stimulation protocol were the same for both LGN and pulvinar sessions.

Figure 2: Sequential or combined visual and electrical stimulation of the LGN (anesthetized animal B06, session *B06fu1*) **(a)** T-statistic maps thresholded at $p < 0.001$ (uncorrected). The cross in the 4th slice shows the location of the electrode tip. **(b)** Time course of the BOLD fMRI responses for the sequential design. Each observation consisted of 5 visual and 5 electrical stimulation trials presented in random order. The leftmost plot shows the average responses of all subcortical structures (subC), i.e. LGN, SC and Pul. The middle four plots depict the time courses of the signal in cortex (conventions as in Fig. 1). The light and dark bars depict the visual and electrical stimulation epochs, respectively. **(c)** Average BOLD responses from all PBR (i.e. subC, V1, MT) and NBR (i.e. V2, XC) regions in the combined stimulus design. Here, the light gray and the patterned bars show the epochs of visual and concurrent visual-electrical stimulation, respectively.

Figure 3: Population BOLD responses to VS and ES of LGN and pulvinar. **(a)** Orthogonal views showing the tip of the electrode for the sessions (N=32) included in the analysis. Red spots are LGN and green spots pulvinar sites. The middle cluster shows the actual 3D position of the recording sites, while the other three clusters depict their projections to the coronal, sagittal and horizontal views of the brain at the level of LGN/pulvinar. **(b)** Three-dimensional reconstructions (top LGN, bottom pulvinar) and **(c)** flat maps for all sessions showing the location and extent of activations/deactivations during electrical stimulation. The top left section of panel **(c)** is an anatomical map showing the gyri and sulci of the posterior cortical region. Int. calc, internal calcarine; operc, operculum; ios, inferior occipital sulcus; ots, occipito-temporal sulcus; lun, lunate; Ips-pos, intraparietal sulcus and parietal occipital sulci; sts, superior temporal sulcus; AngG, angular gyrus. Dashed lines show the bottom of sulci; thick solid white lines the approximate boundaries of visual areas. The top right, bottom left and bottom right maps show activations and deactivations during visual, LGN and pulvinar stimulation, respectively. **(d)** Average time courses for LGN (top) and pulvinar (bottom) stimulation. Each thick line shows the average of the mean responses of each session, while the shaded areas indicate the 1% confidence interval (bootstrap estimate of the mean from 500 samples). **(e)** Frequency of each positive (red) or negative (blue) response in each brain structure. Abbreviations and conventions are as in Fig. 1.

Figure 4: Single-session and population responses to electrical stimulation in alert monkeys. **(a)** T-statistic maps. **(b)** Experimental protocol (see online methods) and time courses of the activated (red) and deactivated (blue) regions in V1 and V2, respectively. **(c)** Responses for 18 sessions. The shaded areas indicate the 1% confidence interval (bootstrap estimate of the mean from 1000 samples). (d) Bar plot showing the average significantly ($p<0.0001$) modulated regions in V1 and V2 over all sessions. Top inset indicates that 95.7% of all significantly modulated V1 voxels show PBR, and 98.2% of all significantly modulated V2 voxels negative BOLD responses.

Figure 5: Effects of stimulation frequency on the BOLD responses (*session B06td1*). **(a)** The upper traces show the typical V1 (red, positive) and V2 (blue, negative) responses during LGN stimulation at 200 Hz frequency (see details in Methods). The inset shows the activated (V1, red) and deactivated (V2, blue) areas. The lower traces show the time courses of the BOLD response for the same areas when the stimulation frequency was set to 12 Hz.

(b) Combined visual and electrical stimulation at 12 Hz. **(c)** BOLD responses in areas V1 and V2 for visual (first epoch) and electrical (2^{nd} – 7^{th} epoch) stimulation at different frequencies (3, 6, 12, 24, 48, 100 and 200 Hz). The inset shows the activity maps. Note that the red and blue curves in this plot correspond to the significantly ($p<0.0001$, uncorrected) modulated response in V1 and V2, respectively, rather than to PBR and NBR.

Figure 6: Typical multiunit responses in V1 to electrical stimulation of LGN. **(a)** Raster plots and peristimulus histograms (PSTHs, 10 ms bin width) for two different animals (F05.nm2 and E04.nm2). A single stimulus pulse (here 450 μA, biphasic, 0.2 ms duration) induced a sequence of excitation followed by a long-lasting inhibition (dashed red line depicts the application of the electrical stimulus). The displayed time frame runs from 100 m before to 400 ms after stimulus presentation. A single experiment consisted of a three epochs (blank-microstimulation-blank) of 5, 45, and 5 seconds duration, respectively. Stimulation frequency was 1 Hz. The blue horizontal lines show the mean spontaneous activity during the prestimulus (first 5 seconds) period. **(b)** The plot shows the principal components, with the highest eigenvalues obtained by single value decomposition (here obtained by svds (response-matrix, 10), Matlab). The choice of the number of clusters was motivated by the observation that over 76% of the signal variance was explained by the first three principal components. **(c)** The plots show the three types of responses obtained by k-means clustering. To optimize clustering the first 10 ms of the responses (masked by the black rectangles), typically a high a peak of excitatory activity, were blocked (strongly attenuated). The first two clusters are inhibitory responses with different durations, and the third cluster comprises short-lived excitatory responses. **(d)** Power of the low (1-40 Hz, thick lines) and high (60-100 Hz, thin lines) frequency ranges of the local field potential (LFP) for the sites and channels clustered on the basis of multiunit activity. **(e)** Mean and standard error of the electrode depth for the recorded sites of each cluster. Clusters 1 and 3 are significantly different at $p<0.0002$. **(f, g)** Pulse efficiency and inter-pulse spiking activity as a function of stimulation frequency (see text).

Figure 7: Analysis of population data. **(a)** Schematic demonstration of the common voxel clusters corresponding to different types of activity changes. The top plot shows the dorso-ventral position of typical slices at and around the electrode tip (the cross in the middle slice). The three subsequent plots illustrate the 4 main regions of interest: INJ, injection; V1, V2; and IPZ, injection projection zone. The bottom plot shows the relative (with respect to the V1 size) size of the ROIs. **(b)** Time course of the signal from each ROI. The red dashed lines indicate the injection time (500 s). The upper plot shows the ES-induced positive and negative BOLD responses in V1 (cyan) and V2 (blue), respectively. The lower plot shows typical time courses within the injected area (INJ, red) and its retinotopically matched V2 location (IPZ, pink). **(c)** The plots show the averages of the first (pre-injection trials 1-13; thin lines) and last (24-37, thick lines) trials for each of the ROIs. Each trial consists of a 32 s ON and a 32 s OFF period. **(d)** Dynamics of response inversion after the injection. Each point is the Pearson coefficient of correlation between the stimulus profile (boxcar convolved with a standard hemodynamic response function) and each trial of the average ROI response.

METHODS

All surgical and experimental procedures were approved by the local authorities (Regierungspraesidium) and were in full compliance with the guidelines of the European Community (EUVD 86/609/EEC) for the care and use of laboratory animals.

General Surgery and Anesthesia All surgical procedures for implantation have been described in detail elsewhere. Briefly, MRI-compatible skull-form-specific head holders and chambers were made out of PEEK (polyether etherketone; TecaPEEK, Ensinger, Inc., Nufringen, Germany) and implanted stereotaxically on the

cranium of each animal using aseptic technique. The implants were secured with custom-made ceramic screws (zirconium oxide Y_2O_3-TPZ 5x1, Pfannenstiel, Germany). Postoperatively, the animals were held in large, specially designed recovery chairs for 3 days, during which time they were taken out for walks by the care persons 2-3 times a day. The chairs allowed the animals to freely move body and hands, but prevented them from touching the implants. As a prophylactic measure, antibiotics (enrofloxacin; Baytril™) and analgesics (Flunixin; Finadyne® vet.) were administered for 3 to 5 days. All surgical procedures were carried out under general balanced anesthesia, the induction and maintenance of which was performed by trained personnel.

Anesthesia for Physiology and fMRI Experiments During the fMRI experiments, anesthesia was maintained with remifentanil (0.5-2 µg/kg/min) in combination with a fast acting paralytic, mivacurium chloride (5-7mg/kg/hr). Because the BOLD signal is very sensitive to changes in body temperature, oxygenation, pH, and blood pressure, the physiological state of the animal was monitored continuously and maintained tightly within normal limits. Body temperature was strictly maintained at 38.5-39.5^{0}C, and end-tidal CO_2 and oxygen saturation were kept constant at 33 mm Hg and over 95%, respectively. Acidosis was prevented by the administration of lactated Ringer's solution with 2.5% glucose, infused at 10 ml/kg/hr, and intravascular volume was maintained by the additional administration of colloids (hydroxyethyl starch, 20-30 ml over 1-2 minutes or 20 ml/kg/hr). To ensure that the absence of a "typical" anesthetic, e.g. isoflurane, desflurane, or propofol, did not cause stress to the animal, we measured catecholamines and optimized dosages to ensure unaffected physiological responses at normal catecholamine concentrations.

Positioning of the Electrode and Microstimulation Recording and microstimulation hardware, including electrodes and microdrives, were developed at the Max Planck Institute for Biological Cybernetics. Recording chambers and head holders were positioned stereotaxically on the basis of individual, high-resolution MRI. On average the chambers for dLGN and pulvinar microstimulation were placed at the coordinates AP=8, ML=12. Stimulation sites were selected so as to ensure reliable electrically evoked BOLD activation on the operculum of the brain. Once the electrode was at the desired location in LGN or pulvinar, we aligned the visual projector and plotted the receptive field of the multiple units. In three animals the stimulation electrodes were implanted chronically to increase efficiency and permit the precise positioning of the injector and the recording electrode in the areas of V1 and V2, respectively. The chronic stimulation electrodes were lowered through a custom-made grid fitted into the recording chamber. After site selection they were permanently fixated, and the grid was sealed with biocompatible silicon (WPI, Sarasota, USA; Kwik-Cast™).

Visual Stimulation (VS) and Electrical Stimulation (ES) Visual stimuli were presented binocularly, initially with an SVGA fiber-optic system (AVOTEC, Silent Vision SV-7021, Stuart, FL) and later with our own custom-made MR-compatible visual stimulator. Both had a spatial resolution of 800x600 pixels and a frame rate of 60 Hz (for details see). Electrical microstimulation was performed with a custom-built constant current source. Current amplitude, pulse duration, train duration and stimulation frequency were controlled digitally using our own TCL-based software and a QNX (Canada) real time operating system. An experiment could have trials of visual (VS) or electrical (ES) stimulation, or trials of alternating (VISESMIX) or combined (VISESCOMB) VS and ES. The VISESMIX trials started with a 10 s blank period followed by 6 s stimulation (rotating checkerboard or microstimulation, randomized within a scan) and a 14 s blank epoch. This sequence was repeated 10 times during an MR scan of 5 min duration. The VISESCOMB design started with a 10 s blank period followed by 10 s visual stimulation (rotating checkerboard), then 10 s of combined visual and electrical stimulation, 10 s visual stimulation alone and finally 10 s blank. This sequence was repeated 6 times during MR scans of 5 min duration. A number of different pulse types were tested to optimize electrical stimulation. Here we present data obtained

with biphasic charge-balanced pulses with 200 μs duration and a frequency of 3 to 200 Hz (pulse train 200 ms on and 200 or 400 ms off). The bulk of the experiments used 100 μm Ir electrodes, with a typical tip surface of A=0.006 mm^2 as measured by electron microscopy after use in an experiment, current I=250 μA, and pulse duration of 200 μs, yielding a charge density of 833 $\mu C/cm^2$. This charge density, which induced robust and highly reproducible cortical activations (V1) and deactivations (extrastriate cortex), is within the range of densities used in many electrostimulation studies, and it is well below that reported to cause tissue damage. For long-lasting (e.g. seven-hour-long) stimulation, for instance, potential histologically verified damage may occur at charge densities exceeding 1600 $\mu C/cm^2$ per phase.

FMRI in Alert Monkeys The scanner, primate chair, and hardware for awake monkey experiments have been described in detail elsewhere. Briefly, the monkeys were positioned in custom-designed primate chairs that have integrated equipment for immobilizing the monkey's head, monitoring jaw and body motions, tracking eye movements, presenting the stimulus, and providing rewards. Electrical stimuli were delivered as described above, via acutely positioned electrodes or a chronically implanted electrode. The experimental paradigm was trial-based: Each trial started after the animal remained motionless for 2 s, at which point a 0.2-0.5 degree fixation spot appeared on the visual stimulation display for a 4 s pre-stimulus period. During this pre-stimulus period the monkey had to fixate and remain motionless. Then, in addition to the fixation spot, a small rotating checkerboard was displayed or the microstimulation pulse train started for 6 s. In the 10 s long post-stimulus period the fixation window was 3-10 degrees. All alert monkey experiments were conducted in a vertical 7 Tesla scanner with a 60 cm diameter bore (BioSpec 7/60v, Bruker BioSpin, Ettlingen, Germany). Radiofrequency coils with 40-60 mm diameter were used as transceivers. For each animal, high-resolution T_1-weighted 3D-MDEFT images were used for anatomical reference. BOLD data were collected with a segmented SE-EPI because of its higher specificity to activation in gray matter and decreased sensitivity to susceptibility artifacts. Acquisition parameters were optimized based on the constraints imposed by the animal's behavior and to reduce susceptibility artifacts. We typically used an FOV of 96x48 mm with a matrix size of 96x48, resulting in a final resolution of 1 mm^2 and a slice thickness of 2 mm. Usually 13 slices were used, oriented in such a way that they covered V1, V2 and LGN. A 2-segment interleaved SE-EPI sequence was used with a receiver bandwidth of 156 kHz, TE 40 ms, TR 1000 ms. A TR of 1000 ms is not optimal for SE; nonetheless its selection was necessitated by the trial length, which in turn was determined by the animal's behavior. Fat suppression was applied where necessary.

FMRI in Anesthetized Monkeys Experiments in anesthetized animals were conducted in a vertical 4.7 Tesla scanner with a 40 cm diameter bore (BioSpec 47/40v, Bruker BioSpin, Ettlingen, Germany). The system has a 50 mT/m (180 μs rise time) actively shielded gradient coil (Bruker, BGA26) with an inner diameter of 26 cm. We used a custom-made chair to position the monkey in the magnet, and customized radiofrequency (RF) coils: an 85mm diameter surface coil or a quadrature volume coil combining a Helmholtz coil and a surface coil on the operculum of the monkey. With the quadrature coil one can image deep brain structures like thalamus while still maintaining high SNR in the primary visual cortex. For the microstimulation experiments, 12 slices were acquired, covering visual cortex and thalamus. BOLD activity from these slices was acquired at a temporal resolution of 2 seconds with four-shot GE-EPI images (TR/TE=500/15ms, bandwidth=100 kHz, FA=30^o, FOV=96x96mm, matrix=96x96, 2mm slice thickness). T1-weighted, high-resolution anatomical scans were obtained using 3D-MDEFT with FOV 96x96x128 mm, matrix 192x192x128 or 256x256x128, TE of 4.5 ms, TR of 15-25 ms, BW 50 kHz, FA of 20 deg, and 4 segments. MRI data were analyzed off-line using our own software developed in MATLAB. Global intensity normalization and signal conditioning were performed prior to statistical map generation. Functional maps were generated using the general linear model (GLM). The functional

maps obtained with GLM were thresholded to identify significantly activated voxels. In addition, a clustering algorithm was applied that eliminated randomly activated voxels. A 5x5 window was centered on each of the activated voxels, and a threshold of 10 co-activated voxels was used to select clusters. In the typical horizontal brain sections displayed in the figures, multiple functionally active areas could be visualized simultaneously. To assign different patterns of positive and negative BOLD responses to different cortical areas, the boundaries of the retinotopically organized areas such as V1, V2, V3, V3A, V4, V4t and MT were identified by mapping vertical meridian activations and consulting anatomical information obtained from our combined MRI and histology atlas of the macaque brain.

Cortical Microinjections of GABA Antagonists GABA antagonists were injected into V1 in experiments combining fMRI, electrophysiological recordings, and microstimulation. GABAergic action was blocked with 10 µl of a 100 µM solution of (-)-bicuculline methiodide (Tocris, Bristol, UK) that was slowly injected into V1 at 1 µl/min, for a total injection duration of 10 minutes. The bicuculline solution was prepared on the basis of artificial cerebrospinal fluid (ACSF) composed of NaCl: 148.19 mM, KCl: 3.0 mM, $CaCl_2$: 1.40 mM, $MgCl_2$: 0.80 mM, Na_2HPO_4: 0.80 mM, NaH_2PO_4: 0.20 mM; all purchased from Sigma-Aldrich (Schnelldorf, Germany). The pH was adjusted with NaOH to 7.25. During injection, flow and volume were monitored by high-precision flow meters (Sensirion, Switzerland). A fused silica glass capillary (outer diameter: 150 µm, inner diameter: 50 µm) that was connected to a custom-made high-precision injection system was positioned within V1 in a region directly affected by the electrical stimulation of LGN. The injections were delivered at depths corresponding to cortical layers IV/V. IPZ was estimated by sparse retinotopic mapping; small rotating polar-checkerboard stimuli were placed in a visual field position that elicited visual BOLD responses around the tip of the injector. The V2 activation induced by such stimuli was considered to be the IPZ. IPZ can also be approximated on the basis of the known retinotopic organization of the early visual areas.

Protocol and Data Analysis for ES and Injection fMRI In the combined ES-injection experiments, cortical BOLD responses were elicited by electrically stimulating LGN for a 32s ON period followed by an OFF period of equal duration without visual stimulation. Each scan consisted of 37 ON/OFF periods, and the GABA antagonist was injected at the end of the eighth OFF period. This experimental design allowed us to examine the effects of an antagonist both on the electrically induced modulation of the BOLD signal and on BOLD baseline signal levels. In such experiments changes in modulation and baseline of the signal during and after the injection cannot be always modeled a priori. Instead, the generation of maps is better accomplished by using unsupervised multivariate data-driven methods of voxel selection. To map the effects of bicuculline on signal propagation we therefore first applied spatial Independent Component Analysis (ICA). Each of the resulting spatial voxel clusters, or independent components, has a time course associated with it. In the present study we were interested exclusively in brain regions that showed a statistically significant activation during the pre-injection period. The calculated ICs were thus further selected by examining the correlation of the time course of each IC cluster with the time course of visual stimulation modeled as a boxcar function convolved with a hemodynamic response function (HRF)[19]. ICA systematically detected clusters around the electrode tip and in the IPZ for all sessions. Finally, activity maps were obtained by using a GLM with a design matrix including the average time course of two ES-related voxel clusters (INJ and IPZ) for all sessions.

Reference List

1. Sultan,F., Augath,M., & Logothetis,N. BOLD sensitivity to cortical activation induced by micro stimulation: comparison to visual stimulation. *Magnetic Resonance Imaging* **25**, 754-759 (2007).

2. Tolias,A.S. *et al.* Mapping Cortical Activity Elicited with Electrical Microstimulation Using FMRI in the Macaque. *Neuron* **48**, 901-911 (2005).

3. Felleman,D.J. & Van Essen,D.C. Distributed Hierarchical Processing in Primate Cerebral Cortex. *Cerebral Cortex* **1**, 1-47 (1991).

4. Logothetis,N.K., Pauls,J., Augath,M., Trinath,T., & Oeltermann,A. Neurophysiological Investigation of the Basis of the fMRI Signal. *Nature* **412**, 150-157 (2001).

5. Goense,J.B. & Logothetis,N.K. Neurophysiology of the BOLD fMRI Signal in Awake Monkeys. *Curr. Biol.* **18**, 631-640 (2008).

6. Friston,K.J. *et al.* Analysis of Fmri Time-Series Revisited. *Neuroimage* **2**, 45-53 (1995).

7. Shipp,S. The functional logic of cortico-pulvinar connections. [129 refs]. *Philosophical Transactions of the Royal Society of London - Series B: Biological Sciences.* **358**, 1605-1624 (2003).

8. Sherman,S.M. The thalamus is more than just a relay. *Current Opinion in Neurobiology* **17**, 417-422 (2007).

9. Shmuel,A., Augath,M., Oeltermann,A., & Logothetis,N.K. Negative Functional MRI Response Correlates with Decreases in Neuronal Activity in Monkey Visual Area V1. *Nature Neuroscience* **9**, 569-577 (2006).

10. Sincich,L.C., Park,K.F., Wohlgemuth,M.J., & Horton,J.C. Bypassing V1: a direct geniculate input to area MT. *Nat. Neurosci.* **7**, 1123-1128 (2004).

11. Butovas,S. & Schwarz,C. Detection psychophysics of intracortical microstimulation in rat primary somatosensory cortex. *European Journal of Neuroscience* **25**, 2161-2169 (2007).

12. Douglas,R.J. & Martin,K.A. A functional microcircuit for cat visual cortex. *J Physiol* **440**, 735-769 (1991).

13. Chung,S. & Ferster,D. Strength and orientation tuning of the thalamic input to simple cells revealed by electrically evoked cortical suppression. *Neuron* **20**, 1177-1189 (1998).

14. Kara,P., Pezaris,J.S., Yurgenson,S., & Reid,R.C. The spatial receptive field of thalamic inputs to single cortical simple cells revealed by the interaction of visual and electrical stimulation. *Proc. Natl. Acad. Sci. U. S. A* **99**, 16261-16266 (2002).

15. Butovas,S., Hormuzdi,S.G., Monyer,H., & Schwarz,C. Effects of electrically coupled inhibitory networks on local neuronal responses to intracortical microstimulation. *Journal of Neurophysiology* **96**, 1227-1236 (2006).

16. Butovas,S. & Schwarz,C. Spatiotemporal effects of microstimulation in rat neocortex: A parametric study using multielectrode recordings. *Journal of Neurophysiology* **90**, 3024-3039 (2003).

17. Logothetis,N.K., Kayser,C., & Oeltermann,A. In Vivo Measurement of Cortical Impedance Spectrum in Monkeys: Implications for Signal Propagation. *Neuron* **55**, 809-823 (2007).

18. Brewer,A.A., Press,W.A., Logothetis,N.K., & Wandell,B.A. Visual Areas in Macaque Cortex Measured Using Functional Magnetic Resonance Imaging. *Journal of Neuroscience* **22**, 10416-10426 (2002).

19. Rauch,A., Rainer,G., & Logothetis,N.K. The Effect of a Serotonin-induced Dissociation between Spiking and Perisynaptic Activity on BOLD Functional MRI. *Proc. Natl. Acad. Sci. U. S. A* **105**, 6759-6764 (2008).

20. Pezaris,J.S. & Reid,R.C. Demonstration of artificial visual percepts generated through thalamic microstimulation. *Proceedings of the National Academy of Sciences of the United States of America* **104**, 7670-7675 (2007).

21. Fries,W. & Distel,H. Large Layer Vi Neurons of Monkey Striate Cortex (Meynert Cells) Project to the Superior Colliculus. *Proceedings of the Royal Society of London Series B-Biological Sciences* **219**, 53-& (1983).

22. Bullier,J. & Henry,G.H. Laminar Distribution of 1St-Order Neurons and Afferent Terminals in Cat Striate Cortex. *Journal of Neurophysiology* **42**, 1271-1281 (1979).

23. Gradinaru,V., Mogri,M., Thompson,K.R., Henderson,J.M., & Deisseroth,K. Optical Deconstruction of Parkinsonian Neural Circuitry. *Science* **324**, 354-359 (2009).

24. Li,C.L. Cortical intracellular synaptic potentials in response to thalamic stimulation. *J Cell Comp Physiol* **61**, 165-179 (1963).

25. Berman,N.J., Douglas,R.J., Martin,K.A., & Whitteridge,D. Mechanisms of inhibition in cat visual cortex. *J Physiol* **440**, 697-722 (1991).

26. Douglas,R.J., Martin,K.A., & Whitteridge,D. An intracellular analysis of the visual responses of neurones in cat visual cortex. *J Physiol* **440**, 659-696 (1991).

27. Okun,M. & Lampl,I. Instantaneous correlation of excitation and inhibition during ongoing and sensory-evoked activities. *Nat. Neurosci.* **11**, 535-537 (2008).

28. Douglas,R.J. & Martin,K.A.C. Recurrent neuronal circuits in the neocortex. *Current Biology* **17**, R496-R500 (2007).

29. Markram,H. *et al.* Interneurons of the neocortical inhibitory system. *Nat. Rev. Neurosci.* **5**, 793-807 (2004).

30. Keller,A. Intrinsic Synaptic Organization of the Motor Cortex. *Cerebral Cortex* **3**, 430-441 (1993).

31. DeFelipe,J., Conley,M., & Jones,E.G. Long-range focal collateralization of axons arising from corticocortical cells in monkey sensory-motor cortex. *J Neurosci.* **6**, 3749-3766 (1986).

32. Berger,T.K., Perin,R., Silberberg,G., & Markram,H. Frequency-dependent disynaptic inhibition in the pyramidal network: a ubiquitous pathway in the developing rat neocortex. *Journal of Physiology-London* **587**, 5411-5425 (2009).

33. Tehovnik,E.J., Slocum,W.M., Carvey,C.E., & Schiller,P.H. Phosphene induction and the generation of saccadic eye movements by striate cortex. *Journal of Neurophysiology* **93**, 1-19 (2005).

34. Salzman,C.D., Murasugi,C.M., Britten,K.H., & Newsome,W.T. Microstimulation in visual area MT: effects on direction discrimination performance. *J Neurosci.* **12**, 2331-2355 (1992).

35. Murphey,D.K. & Maunsell,J.H.R. Behavioral detection of electrical microstimulation in different cortical visual areas. *Current Biology* **17**, 862-867 (2007).

36. Lehky,S.R. & Sejnowski,T.J. Network model of shape-from-shading: neural function arises from both receptive and projective fields. *Nature* **333**, 452-454 (1988).

37. Moeller,S., Freiwald,W.A., & Tsao,D.Y. Patches with links: A unified system for processing faces in the macaque temporal lobe. *Science* **320**, 1355-1359 (2008).

38. Moore,T., Armstrong,K.M., & Fallah,M. Visuomotor origins of covert spatial attention. *Neuron* **40**, 671-683 (2003).

39. Moore,T. & Armstrong,K.M. Selective gating of visual signals by microstimulation of frontal cortex. *Nature* **421**, 370-373 (2003).

40. Armstrong,K.M., Fitzgerald,J.K., & Moore,T. Changes in visual receptive fields with microstimulation of frontal cortex. *Neuron* **50**, 791-798 (2006).

41. Stanton,G.B., Bruce,C.J., & Goldberg,M.E. Topography of Projections to Posterior Cortical Areas from the Macaque Frontal Eye Fields. *Journal of Comparative Neurology* **353**, 291-305 (1995).

42. Schall,J.D., Morel,A., King,D.J., & Bullier,J. Topography of Visual-Cortex Connections with Frontal Eye Field in Macaque - Convergence and Segregation of Processing Streams. *Journal of Neuroscience* **15**, 4464-4487 (1995).

43. Ruff,C.C. *et al.* Concurrent TMS-fMRI and psychophysics reveal frontal influences on human retinotopic visual cortex. *Current Biology* **16**, 1479-1488 (2006).

44. Ekstrom,L.B., Roelfsema,P.R., Arsenault,J.T., Bonmassar,G., & Vanduffel,W. Bottom-up dependent gating of frontal signals in early visual cortex. *Science* **321**, 414-417 (2008).

45. Ekstrom,L.B., Roelfsema,P.R., Arsenault,J.T., Kolster,H., & Vanduffel,W. Modulation of the Contrast Response Function by Electrical Microstimulation of the Macaque Frontal Eye Field. *Journal of Neuroscience* **29**, 10683-10694 (2009).

46. Guillery,R.W. Anatomical evidence concerning the role of the thalamus in corticocortical communication: A brief review. *Journal of Anatomy* **187**, 583-592 (1995).

47. Cowey,A. The Ferrier Lecture 2004 - What can transcranial magnetic stimulation tell us about how the brain works? *Philosophical Transactions of the Royal Society B-Biological Sciences* **360**, 1185-1205 (2005).

48. Hallett,M. Transcranial magnetic stimulation: A primer. *Neuron* **55**, 187-199 (2007).

49. Allen,E.A., Pasley,B.N., Duong,T., & Freeman,R.D. Transcranial magnetic stimulation elicits coupled neural and hemodynamic consequences. *Science* **317**, 1918-1921 (2007).

50. Driver,J., Blankenburg,F., Bestmann,S., Vanduffel,W., & Ruff,C.C. Concurrent brain-stimulation and neuroimaging for studies of cognition. *Trends Cogn Sci.* **13**, 319-327 (2009).

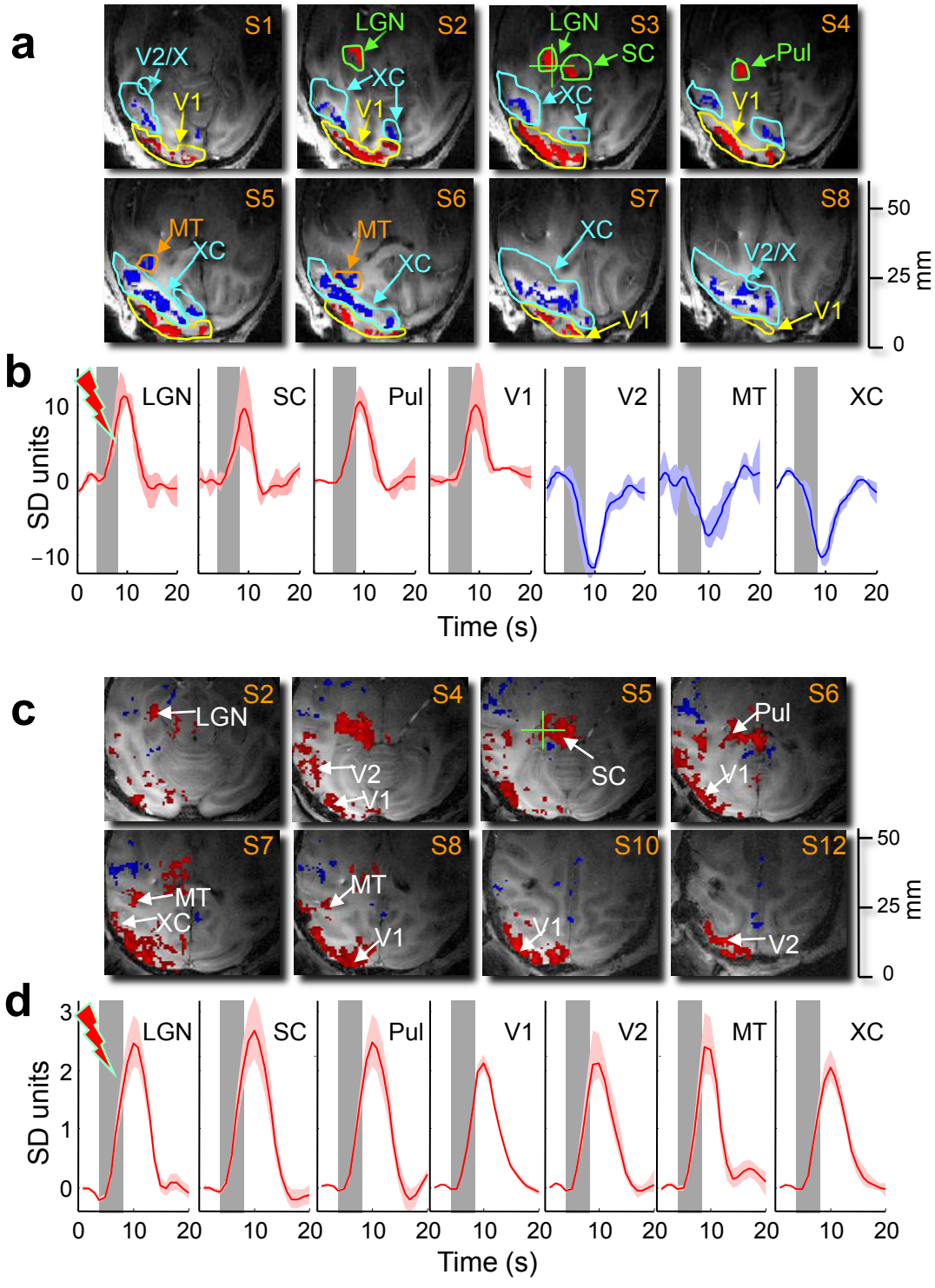

Figure 1

Logothetis et al, Nature Neuroscience 2010.

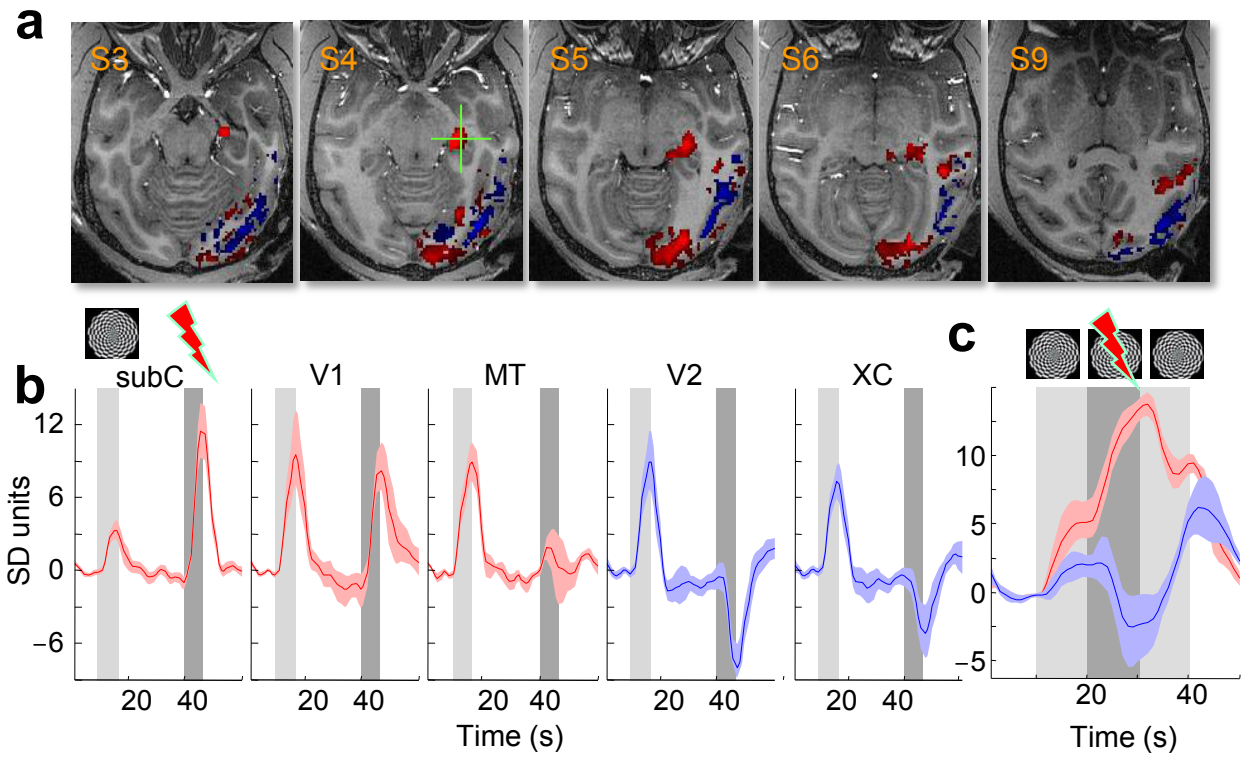

Figure 2

Logothetis et al, Nature Neuroscience 2010.

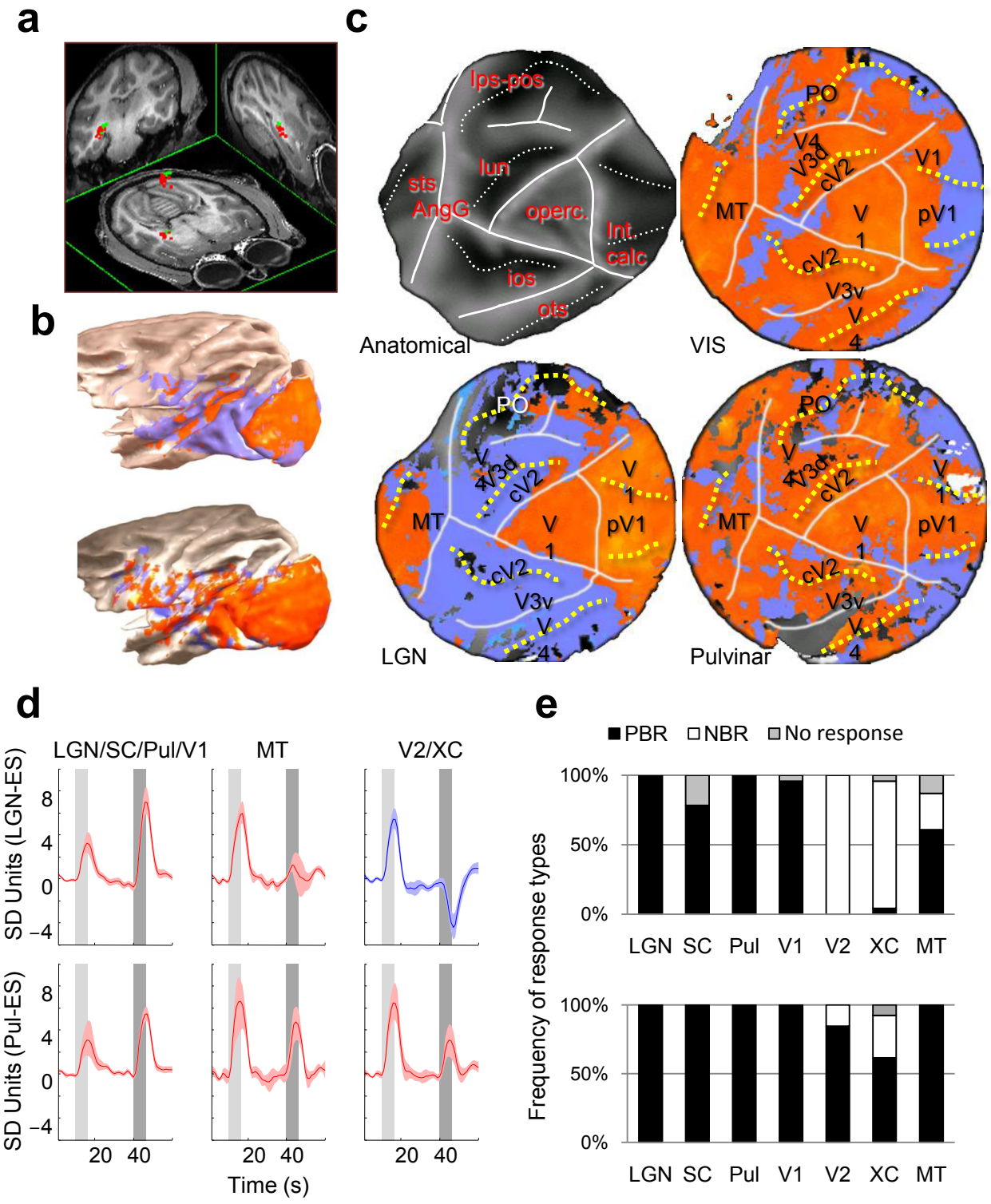

Figure 3

Logothetis et al, Nature Neuroscience 2010.

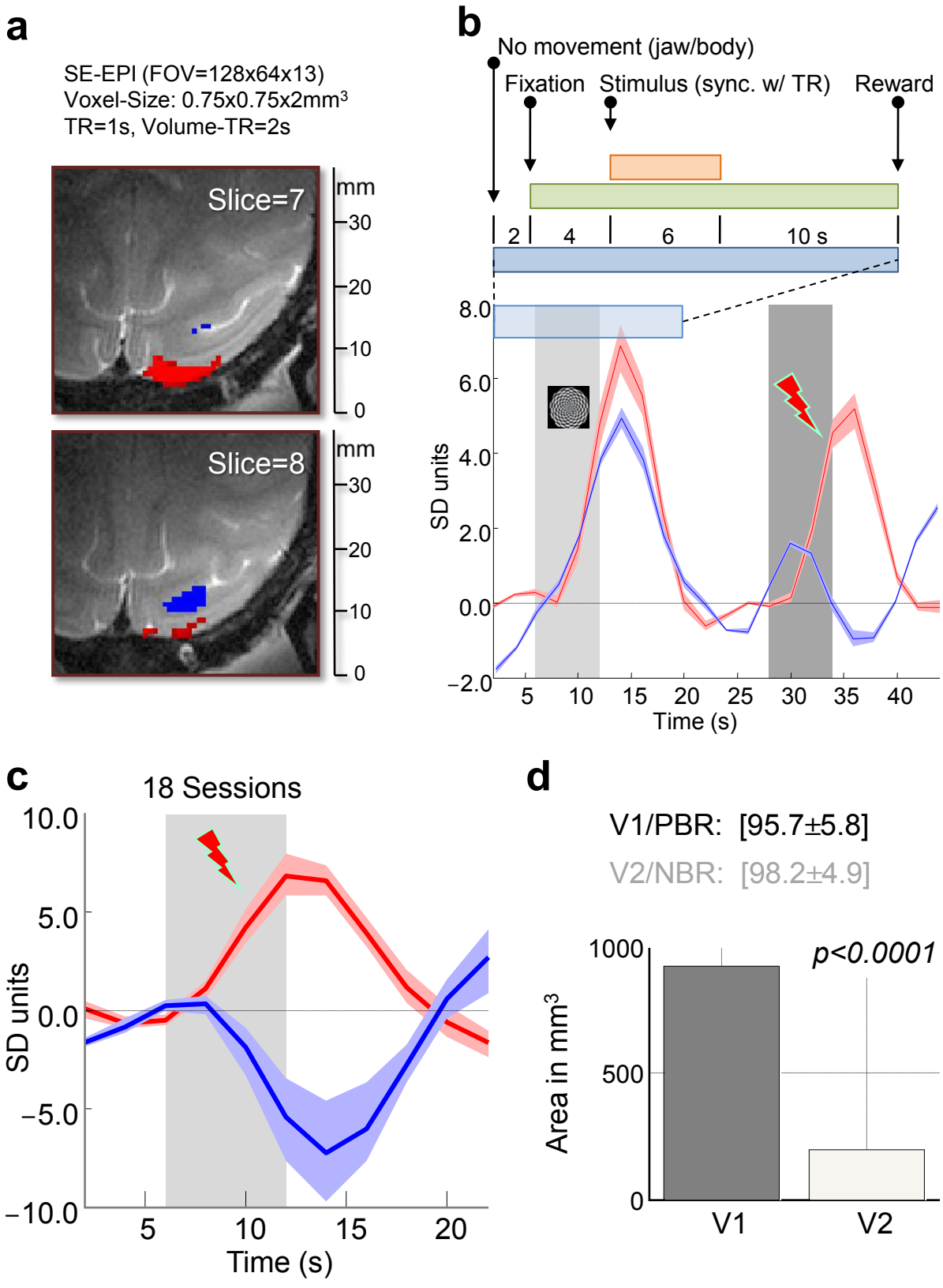

Figure 4

Logothetis et al, Nature Neuroscience 2010.

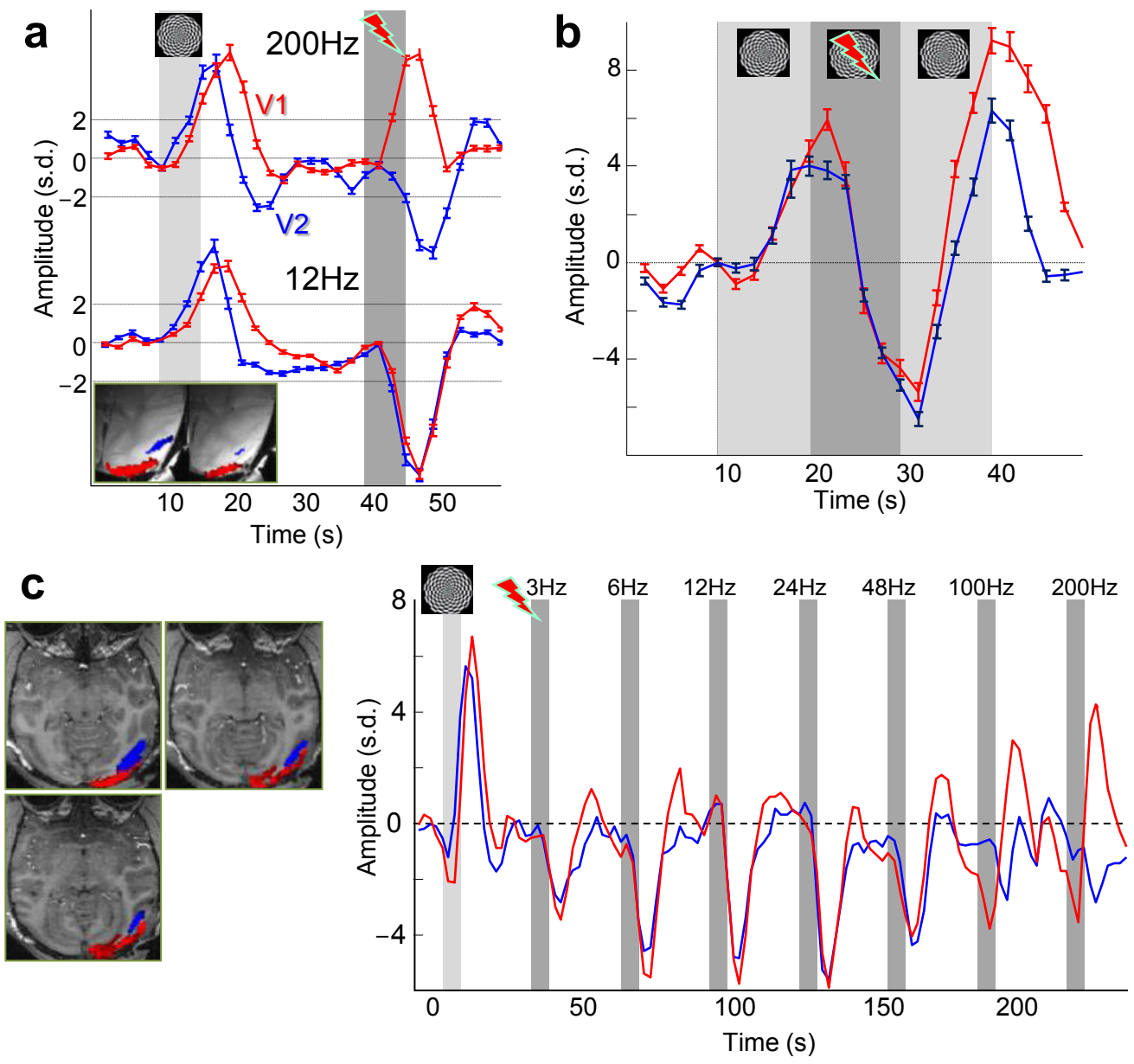

Figure 5

Logothetis et al, Nature Neuroscience 2010.

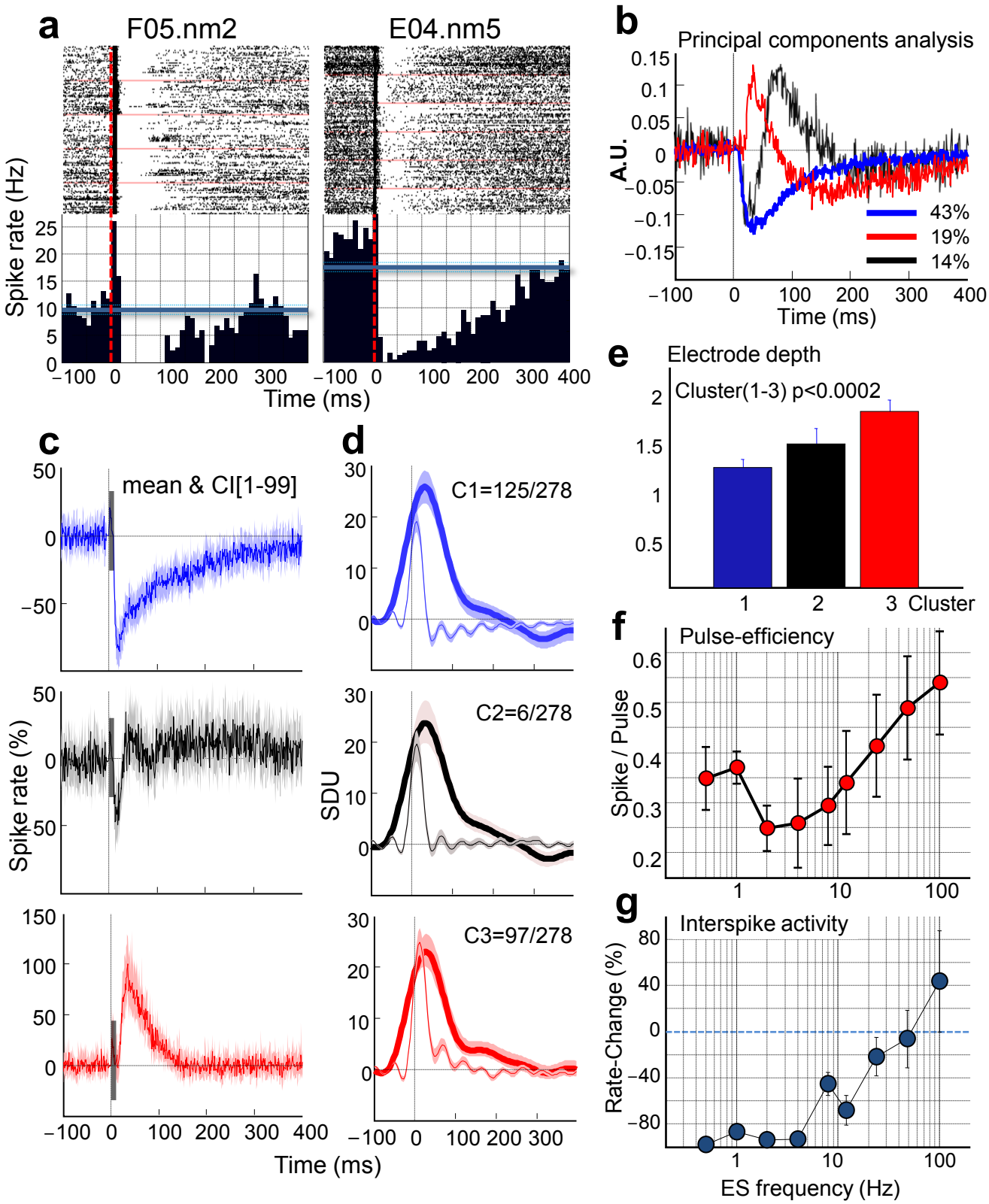

Figure 6

Logothetis et al, Nature Neuroscience 2010.

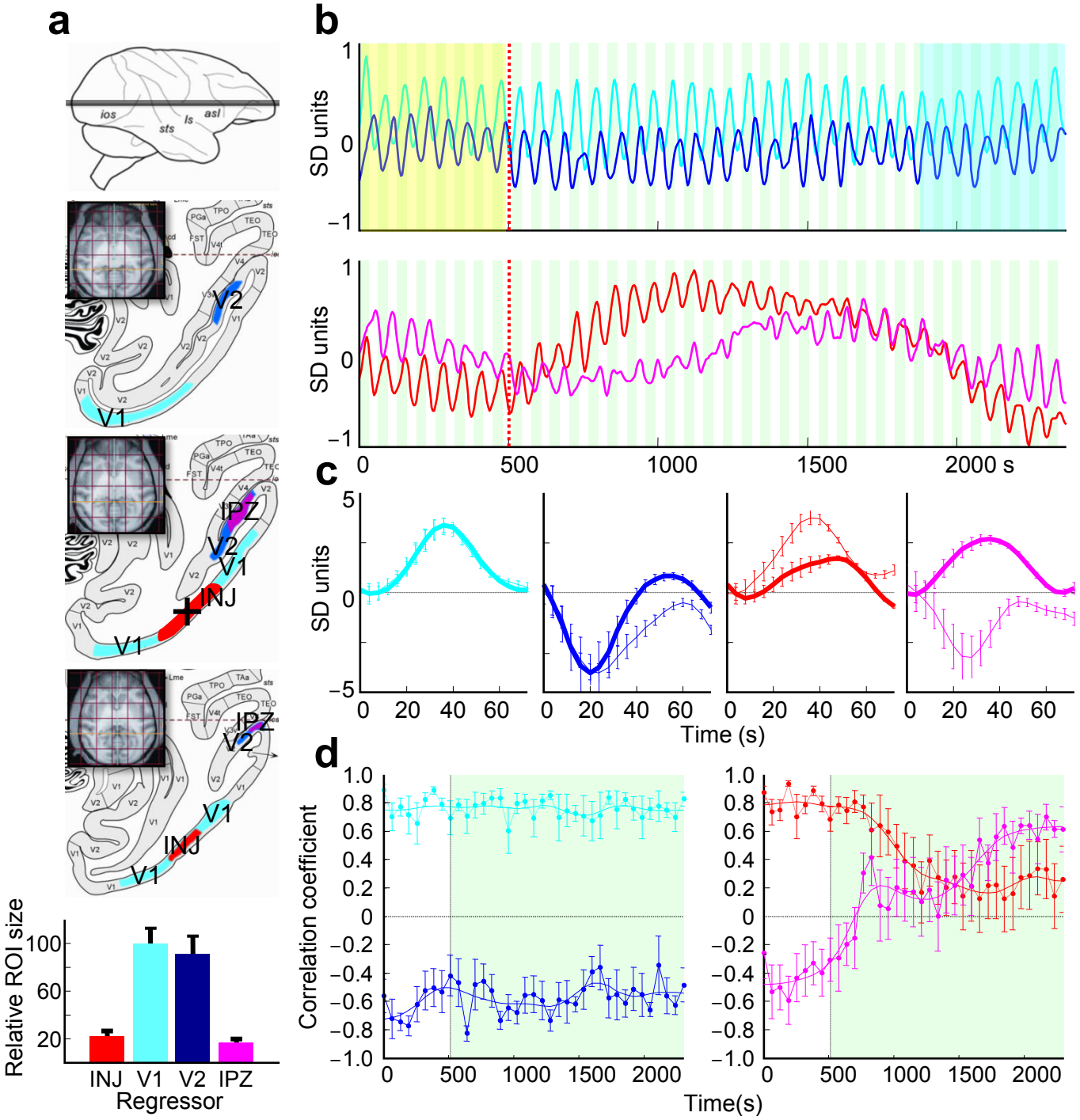

Figure 7

Logothetis et al, Nature Neuroscience 2010.